Variable Angle Asymmetric Cut Monochromator.*

R.K. Smither and P.B. Fernandez
Experimental Facilities Division
Advanced Photon Source
Argonne National Laboratory
Argonne Il 60439

September, 1993

jw

*This work supported by the U.S. Department of Energy, BES-Materials Sciences, under contract no. W-31-109-ENG-38

Poster No. L7 Presented at the SRI conference held at NIST in Gaithersburg, MD, August 22-26, 1993

Variable Angle Asymmetric Cut Monochromator*

R. K. Smither and P. B. Fernandez
Advanced Photon Source
Argonne National Laboratory
Argonne, IL 60439

Variable Angle Asymmetric Cut Monochromator*

R. K. Smither and P. B. Fernandez
Advanced Photon Source
Argonne National Laboratory
Argonne, IL 60439

Abstract

A variable incident angle, asymmetric cut, double crystal monochromator was tested at Argonne National Laboratory to evaluate its possible use on beamlines at the Advanced Photon Source (APS). For both undulator and wiggler beams the monochromator can expand the area of the footprint of the beam on the surface of the crystals to 50 times the area of the incident beam. This increase in area will reduce the slope errors by a factor of 2500. The asymmetric cut allows one to increase the acceptance angle for incident radiation and obtain a better match to the opening angle of the incident beam. This can increase the intensity of the diffracted beam by a factor of 2 to 5 and can make the beam more monochromatic, as well. The monochromator consists of two matched, asymmetric cut (18 degrees), silicon crystals mounted so that they can be rotated about three independent axes. Rotation around the first axis controls the Bragg angle. The second rotation axis is perpendicular to the diffraction planes and controls the increase of the area of the footprint of the beam on the crystal surface. Rotation around the third axis controls the angle between the surface of the crystal and the wider, horizontal axis for the beam and can make the footprint a rectangle with a minimum length for this area. The asymmetric cut is 18 degrees for the matched pair of crystals, which allows one to expand the footprint area by a factor of 50 for Bragg angles up to 19.15 degrees (6 keV for Si[111] planes). This monochromator, with proper cooling, will be quite useful for analyzing the high intensity x-ray beams produced by both undulators and wigglers at the APS.

*This work is supported by the U.S. DOE Contract No. W-31-109-Eng-38.

INTRODUCTION

A considerable amount of research effort has been expended at Argonne National Laboratory and at other synchrotron laboratories around the world to solve the high heat load problem that will exist at the new third generation synchrotron sources.[1-5] The high heat load problem for the first optical component (diffraction crystal, multilayer, mirror, etc.)in the beam line is particularly sever for the new insertion device sources where the x-ray beam flux per unit area and the total power will be 10 to 100 times what is presently available.[6]

A number of partial solutions to this high heat load problem have been developed that improve the cooling of the first optical element, i.e. Argonne has pioneered the use of liquid metal cooling.[1-5]

After one has implemented the best cooling system possible, the most efficient way to further reduce the distortions of the surfaces of the first optical elementis is to spread out the foot print of the x-ray beam. A novel geometry for a double crystal monochromator that spreads the x-ray beam out in the direction perpendicular to the beam direction has been developed for undulator beams at Argonne.[5] This "high tilt" geometry has been tested and works well for undulator beams that are quite narrow in the direction perpendicular to the beam, usually only a few millimeters wide, but does not work well for wiggler beams that tend to be mueh wider (2 to 6 cm). The work presented in this paper describes the design and preliminary lab tests of a double crystal monochromator that will work well for both wiggler and undulator beams.

DESIGN AND SPECIAL FEATURES

The new double-crystal monochromator consists of two 18-degree asymmetric-cut silicon crystals, using the (111) planes. Each crystal can be rotated around three independent axes, as shown in Figure 1. α_m is the asymmetric-cut angle (i.e.,18 degrees). α, is the angle between the crystalline planes and the surface of the crystal in the direction of the beam. σ is the angle between the crystalline planes and the surface of the crystal perpendicular to the beam direction. γ is the angle between the crystal surface and the beam direction (i.e., $\gamma = \theta - \alpha$) Rotation around the first axis changes the Bragg angle (θ) of the incident x-ray beam with the crystalline planes. Rotation around the second axis (ϕ), which is perpendicular to the first, changes the size of the footprint of the beam on the surface of the diffraction crystal by changing the effective asymmetric cut of the crystal, which in tern changes the angle between the incident beam and the surface of the crystal. Rotation around the third axis (ψ, which is perpendicular to the first two, changes the shape of the footprint and allows one to expand the area of the footprint to the maximum area possible for any given crystal size. The salient features of this design are:

1. Variable beam footprint for high heat load applications: An increase in the area of the footprint by a factor 25 to 50 relative to the incident beam will reduce the slope errors caused by the heat in the x-ray beam by a factor of 625 to 2500, respectively.

2. Variable acceptance: The angular and energy acceptance for each crystal can be adjusted for maximum throughput. An increase in the throughput of the monochromator of 2 to 5 can be achieved.

3. Reduced vertical walk: The vertical displacement of the output beam that occurs with a change in the Bragg angle is significantly reduced compared to the vertical walk of the output beam of a standard double crystal monochromator.

4. Increased monochromatic nature of the output beam: A factor of two decrease in the FWHM of the diffracted energy spectrum is possible.

VARIABLE FOOTPRINT

The area expansion ratio, R, is the ratio of the footprint area on the crystal surface to the cross-section area of the incident beam. $R = 1/[\sin\gamma\cos(\sigma-\psi)]$, where $\gamma = \theta - \alpha$, $\tan\alpha = \tan\alpha_m \sin\phi$, and $\tan\sigma = \tan\alpha_m \cos\phi$. The shape of the footprint is shown in figure 2 where $L_0 = H/\sin\gamma$, $L_S = W \tan(\sigma-\psi) \cos\theta/\sin\gamma$ and $W_f = W/\cos(\sigma-\psi)$. H and W are the vertical and horizontal dimensions of the incident beam. The area of the footprint is $L_0 \times W_f$, and the total length of the footprint along the beam direction is $L_0 + L_S$. By adjusting $\psi = \sigma$, we can make $L_S = 0$ and minimize the length of the footprint.

Figure 3 shows some results obtained at Argonne with a 4-mm-high and 12-mm-wide x-ray beam with an energy of 8 keV ($\theta = 14.2^o$), as one changes ϕ and ψ. The shortest footprint for an expansion ratio of 13.8 is obtained with ϕ at 34^o and ψ between 10^o and 14^o. Figure 4 shows some experimental results obtained with an APS-undulator-shape x-ray beam, 1 mm high and 2 mm wide, with an energy of 8 keV (Bragg angle, $\theta = 14.2^o$), as one changes ϕ, with ψ fixed at 14^o. Note that the extra length that is added by the parallelogram shape (sloping ends) does not add much to the

overall length of the footprint. This means that ψ need not be varied during the experiment as the footprint size is changed and/or as the energy of the beam is changed,. This effect is illustrated in the calculations shown in figure 5 in which ψ is fixed at 14° for all cases, and R_A, the increase in footprint area relative to the incident beam area, is held close to 50. Figure 6 shows a similar calculation for an APS-wiggler-shaped beam, in which R is held close to 25.

ANGLE AND ENERGY ACCEPTANCE

The angle acceptance and the energy bandwidth of the asymmetric cut monochromator can be varied by changing the angle ϕ, the rotation around the axis perpendicular to the crystalline planes. This changes the incident angle γ of the x-ray beam on the surface of the crystal and the effective asymmetric cut angle α and the value of the parameter "b" where "b" = $\sin(\theta-\alpha) / \sin(\theta+\alpha)$. The shape of the beam is also changed. The vertical height H_{bp} is increased over the height of the incident beam H_s by a factor of "1/b" as is shown in figure 7. The angular acceptance of the first crystal for diffraction of a monochromatic beam varies as $1/(b)^{0.5}$. The angular emittance of the first crystal varies as $(b)^{0.5}$ for a monochromatic beam. Thus, the ratio of the angular emittance of the diffracted beam to the angular acceptance of the incident beam is given by the value of b. This effect is illustrated in figure 8, in which the acceptance angle of the asymmetric crystal is compared with the acceptance angle of a symmetric crystal. The asymmetric case assumes that the incident angle of the beam on the surface of the crystal (γ) is adjusted to be equal to 2.29 degrees at all energies. This has the effect of keeping the expansion of the footprint at 25 times the area of the incident beam.

Figure 9 illustrates this increase in acceptance angle for positive values of ϕ, for the Cu K-$M_{II}M_{III}$ x-ray doublet. The intensity of the diffracted beam from the first crystal (filled circles) and the intensity of the diffracted beam from the second crystal (open squares) are plotted as a function of the angle ϕ. ψ is fixed at 14°. About 80 percent of the diffracted beam from the first crystal is recovered by the second crystal. Further improvement in this recovery ratio can be obtained by reducing the value of ϕ for the second crystal which increases the acceptance of the second crystal and brings the recovery of the intensity of the first crystal

by the second crystal to almost 100 percent. This effect is illustrated in figure 9, where the open circle data points at ϕ= 30° and 35° are the intensities of the diffracted beam from the second crystal when the value of ϕ is reduced from 30° to 23° and from 35° to 26°, respectively. This control over the acceptance angle of the two crystals can be used to vary the monochromatic nature of the output beam as well as its size, shape and angular divergence.

VERTICAL WALK

The calculations were performed for an offset between the two crystals of X_0 = 20 mm and zero vertical displacement with a zero displacement set at 8 keV, θ = 14.3 degrees and the area expansion ratio R= 25 (see figure 10). The vertical walk for angles +/- 5 degrees was 0.2 to 0.1 of that for the normal symmetric cut monochromator. This effect occurs because the exit angle of the x-ray beam relative to the surface of the crystal is much less in the asymmetric case than in the symmetric case. The walk along the surface of the second crystal is also less. The asymmetric configuration has two advantages over the normal geometry. First, it allows for a larger rotation in θ before a translation of the second crystal is required to correct for the vertical displacement of the beam. Second, the vertical displacement adjustment is less sensitive to errors in the translation of the second crystal along the beam direction.

References

1. R. K. Smither, G. A. Forster, C. A. Kot, and T. M. Kuzay, Liquid Gallium Metal Cooling for Optical Elements with High Heat Loads, Nucl. Instrum. Meth. **A266** (1988) 517-524.

2. R. K. Smither, G. A. Foster, D. H. Bilderback, M. Bedzyk, K. Finkelstein, C. Henderson, J. White, L. E. Berman, P. Stefan, and T. Oversluizen, Liquid Gallium Cooling of Silicon Crystals in High Intensity Photon Beams, Rev. Sci. Instrum. **60** (1989) 1486-1492.

3. R. K. Smither, Use of Liquid Metals as Cooling Fluids, Workshop on High Heat Load X-Ray Optics, ANL/APS/TM-6 (Aug. 1989) 83-131.

4. R. K. Smither, W. Lee, A. Macrander, D. Mills, and S. Rogers, Recent

Experiments with Liquid Gallium Cooling of Crystal Diffraction Optics, paper presented at the 4th International Conference on Synchrotron Radiation Instrumentation, July 15-19, 1991, in Chester, England. Published in Rev. Sci. Instrum. 63 (1992) 485, and Rev. Sci. Instrum., 63 (1992) 1746-1754.

5. W. K. Lee, A. T. Macrander, D. M. Mills, C. S. Rogers and R. K. Smither, Performance of a Gallium-Cooled 85° Inclined Silicon Monochromator for a High Power Density X-Ray Beam, Nucl Instrum. & Meth. Phys. Res. A320 (1992) 381-387.

6. P.J. Viccaro, Power Distribution from Insertion Device Synchrotron X-Ray Sources, SPIE 1990 Intl. Symposium On Opt., 7/90, San Diego, CA

Figure Captions

Figure 1. Schematic drawing of an asymmetric cut crystal showing three axes of rotation and associated angles

Figure 2. Footprint of x-ray beam on asymmetric-cut crystal and associated dimensions.

Figure 3. Experimentally observed shapes of the x-ray beam footprint on the asymmetric-cut crystals with variation of ϕ and ψ. Initial beam, 4 mm high and 12 mm wide, (and final beam profiles) are shown on the left.

Figure 4. Calculated variation of the size and shape of the footprint for an undulator-shaped beam (height = 1 mm, width = 2 mm) with changes in energy and Bragg angle, with the adjustment of ϕ to keep the increased area ratio near 25, and with a constant value of ψ fixed at 14°.

Figure 5. Calculated variation of the size and shape of the footprint for an undulator-shaped beam (height = 1 mm and width = 2 mm) with changes in energy and Bragg angle, with the adjustment of ϕ to keep the increased area ratio near 50, and with ψ fixed at 14°.

Figure 6. Calculated variation of the size and shape of the footprint for an

wiggler-shaped beam (height = 2.3 mm and width = 40 mm) with changes in energy and Bragg angle and the adjustment of ϕ to keep the increased area ratio near 25, and with ψ fixed at 14°.

Figure 7. Schematic view of the asymmetric-cut two-crystal monochromator.

Figure 8. Comparison of the acceptance angle of the first crystal in the asymmetric cut (solid line) and a normal symmetric cut (dashed line) crystal monochromators.

Figure 9. The intensity of the diffracted beam from the first crystal as a function of ϕ for the Cu K-$M_{II}M_{III}$ doublet, for the case when $\psi = 14°$ (open squares). The intensity for the diffracted beam from the second crystal as a function of ϕ is shown (solid circles) for comparison.

Figure 10. Comparison of the vertical walk of a normal two-crystal monochromator with that of the asymmetric-cut two-crystal monochromator as the Bragg angle is changed.

INFRARED
CAMERA

SILICON
CRYSTAL

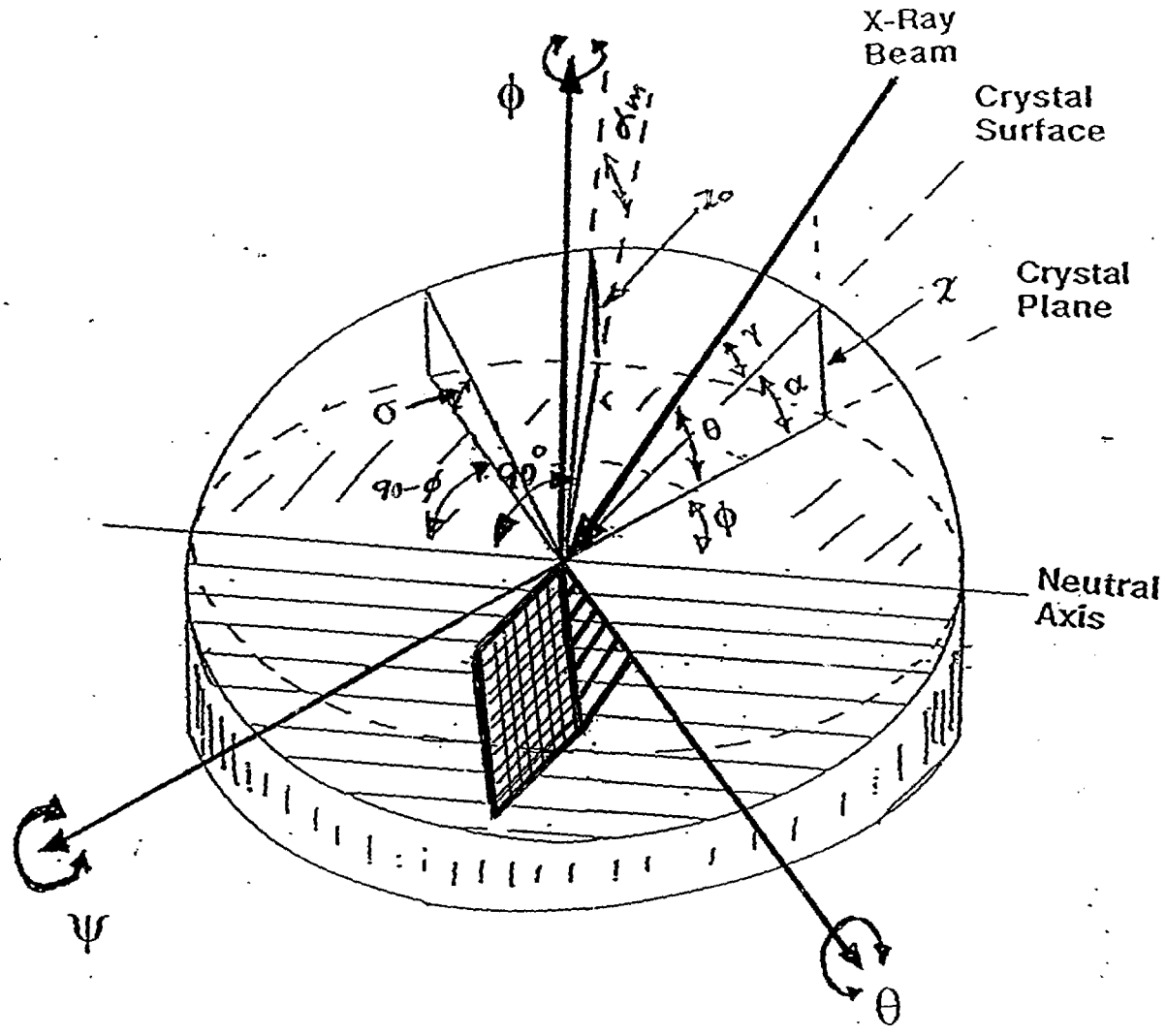
X-Ray
Beam
Crystal
Surface
Crystal
Plane
Neutral
Axis
ϕ
δ
z_0
χ
γ
α
θ
σ
$90-\phi$
90°
ϕ
ψ
θ

Fig 1

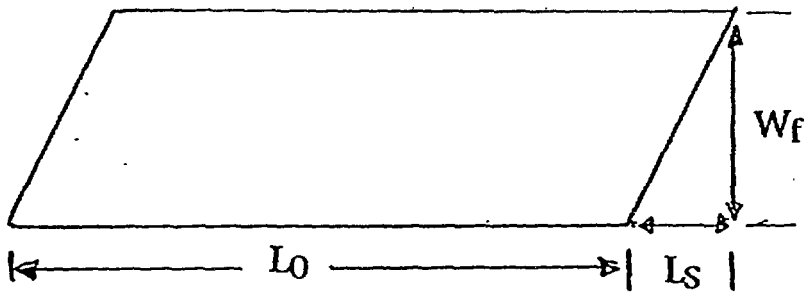

FIG 2

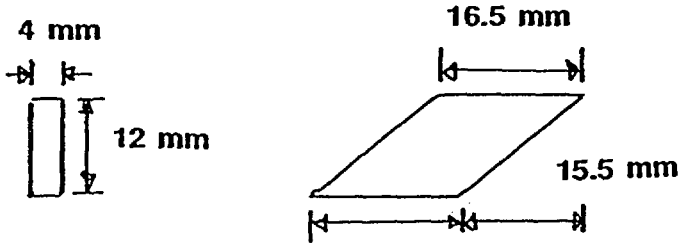

$\Theta = 14.2^{o}$ $\phi = 0^{o}$ $\psi = 0^{o}$

AREA RATIO = 4.2 : 1
LENGTH = 32 mm

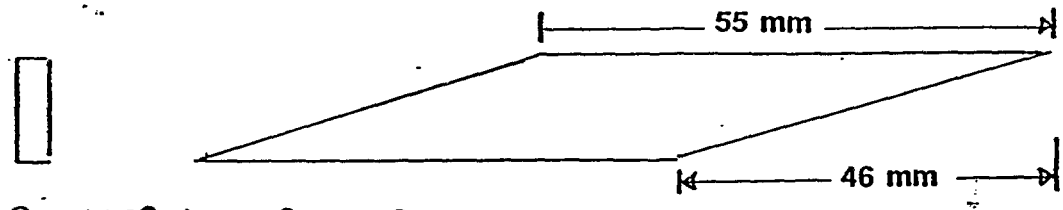

$\Theta = 14.2^{o}$ $\phi = 34^{o}$ $\psi = 0^{o}$

AREA RATIO = 14.3 : 1
LENGTH = 101 mm

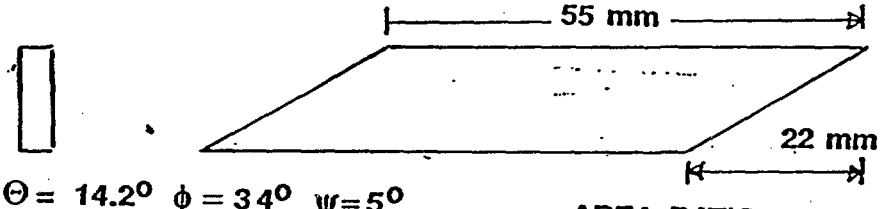

$\Theta = 14.2^{o}$ $\phi = 34^{o}$ $\psi = 5^{o}$

AREA RATIO = 14.0 : 1
LENGTH = 77 mm

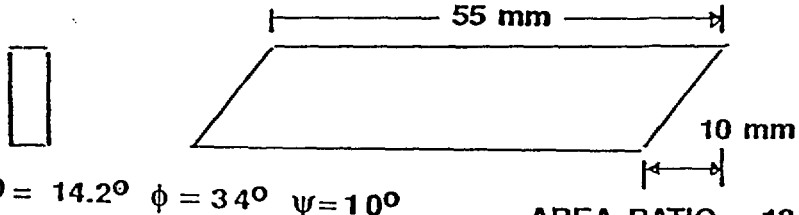

$\Theta = 14.2^{o}$ $\phi = 34^{o}$ $\psi = 10^{o}$

AREA RATIO = 13.8 : 1
LENGTH = 65 mm

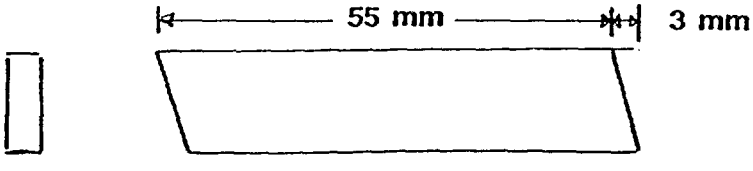

$\Theta = 14.2^{o}$ $\phi = 34^{o}$ $\psi = 15^{o}$

AREA RATIO = 13.8 : 1
LENGTH = 58 mm

Fig 3

$\Theta = 14.2^{o}$ $\phi = 40^{o}$ $\psi = 14^{o}$ AREA RATIO = 24 : 1
LENGTH = 48 mm

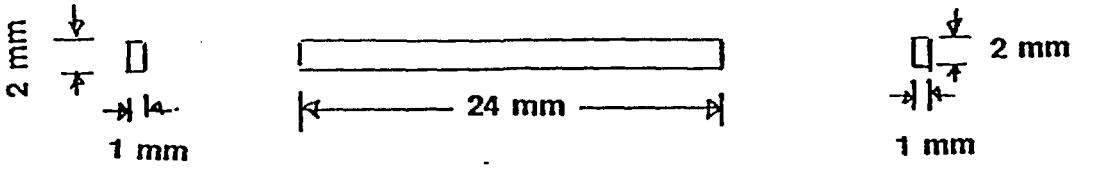

$\Theta = 14.2^{o}$ $\phi = 43^{o}$ $\psi = 14^{o}$ AREA RATIO = 33: 1
LENGTH = 33 mm

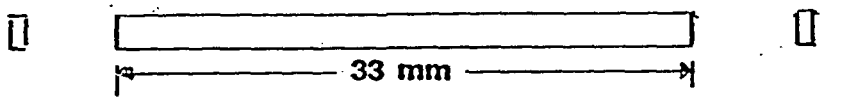

$\Theta = 14.2^{o}$ $\phi = 44^{o}$ $\psi = 14^{o}$ AREA RATIO = 38 : 1
LENGTH = 39 mm

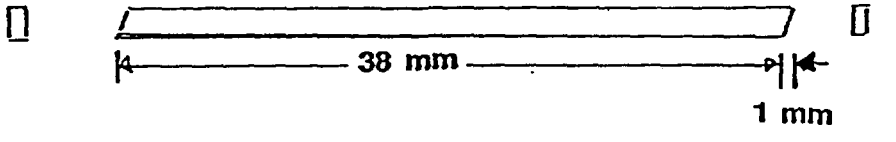

$\Theta = 14.2^{o}$ $\phi = 46^{o}$ $\psi = 14^{o}$ AREA RATIO = 50 : 1
LENGTH = 52 mm

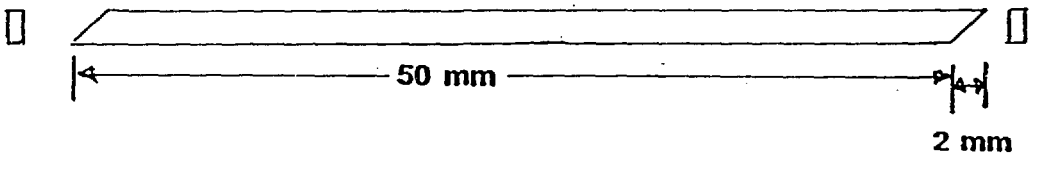

Fig 4

θ	Energy		ϕ	$L_o + L_s$	R_A
2.2°	51.3 keV	9 mm, 50 mm	3.3°	59.0 mm	50.2
4.2°	26.9 keV		9.5°	58.6 mm	50.2
6.2°	18.2 keV		16.8°	57.9 mm	50.1
8.2°	13.8 keV		22.4°	56.7 mm	50.1
10.2°	11.1 keV		29.4°	55.1 mm	50.1
12.2°	9.2 keV		37.0°	53.0 mm	50.0
14.2°	8.0 keV	50 mm	45.5°	50.0 mm	50.0
15.2°	7.5 keV		50.4°	51.9 mm	50.0
16.2°	7.1 keV		55.9°	54.2 mm	50.0
17.2°	6.7 keV		62.3°	57.1 mm	50.1
18.2°	6.2 keV	11, 50 mm	70.8°	61.1 mm	50.3
19.2°	6.0 keV	21, 48 mm	90.0°	68.4 mm	49.0
20.2°	5.7 keV	11, 38 mm	90.0°	49.5 mm	39.4

Fig 5

Ψ = 13.83° Width of Beam = 4 cm Height of Beam = 2.3 mm

Lo + Ls (mm)	ϕ (deg.)	R		Θ (deg.)	Energy (KeV)
128.7	9.9°	25.1	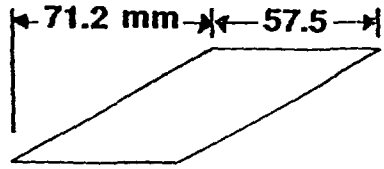	4.2°	26.90
114.3	18.6°	25.1	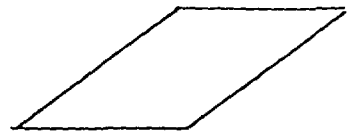	8.2°	13.81
92.2	32.5°	25.0	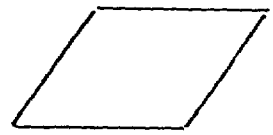	12.2°	9.23
57.5	40.7°	25.0	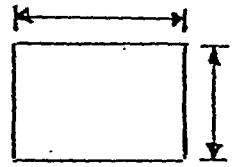	14.2°	8.03
90.3	49.7°	25.0	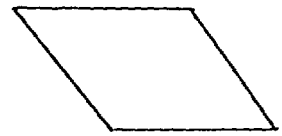	16.2°	7.06
112.3	55.0°	25.0	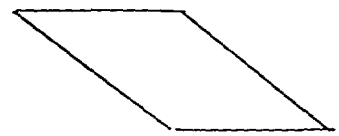	17.2°	6.66
140.1	61.3°	25.1	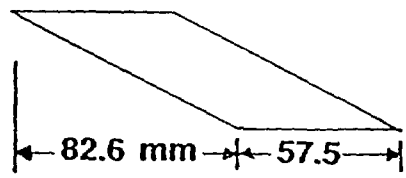	18.2°	6.31

Fig. 6

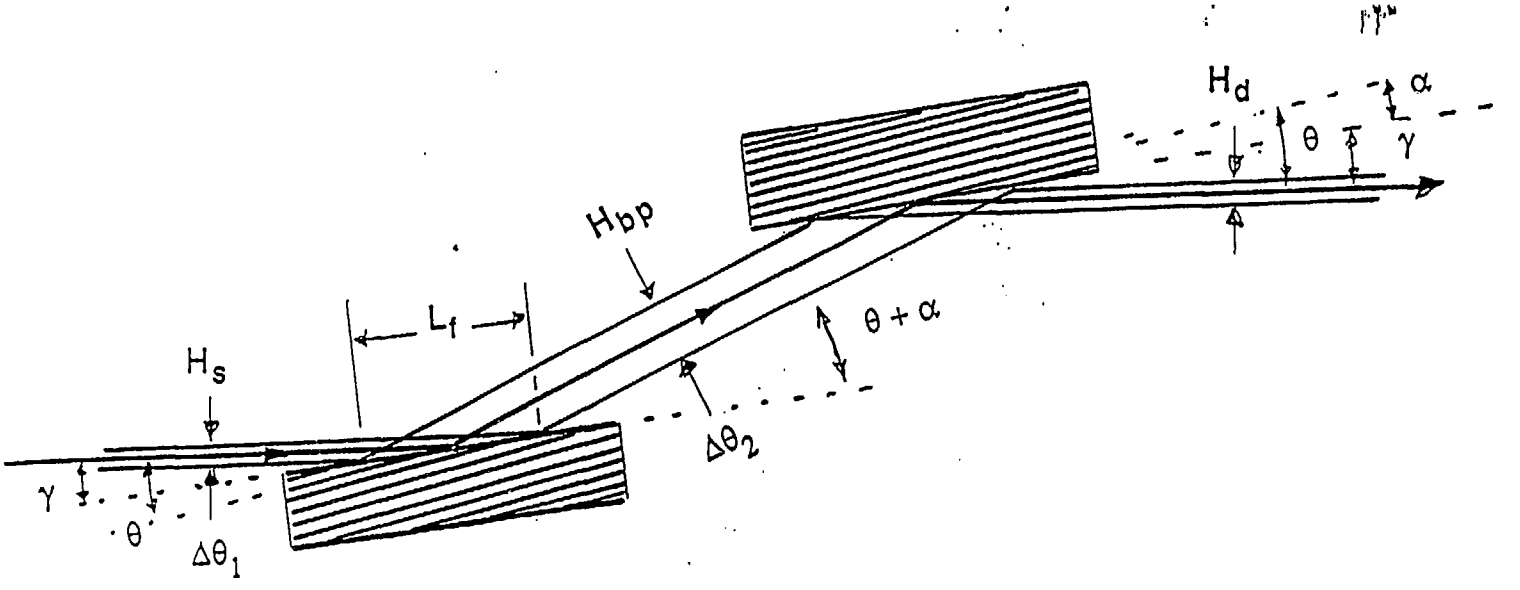
H_d
α
θ
γ
H_{bp}
L_f
$\theta+\alpha$
H_s
$\Delta\theta_2$
γ
θ
$\Delta\theta_1$

Fig 7

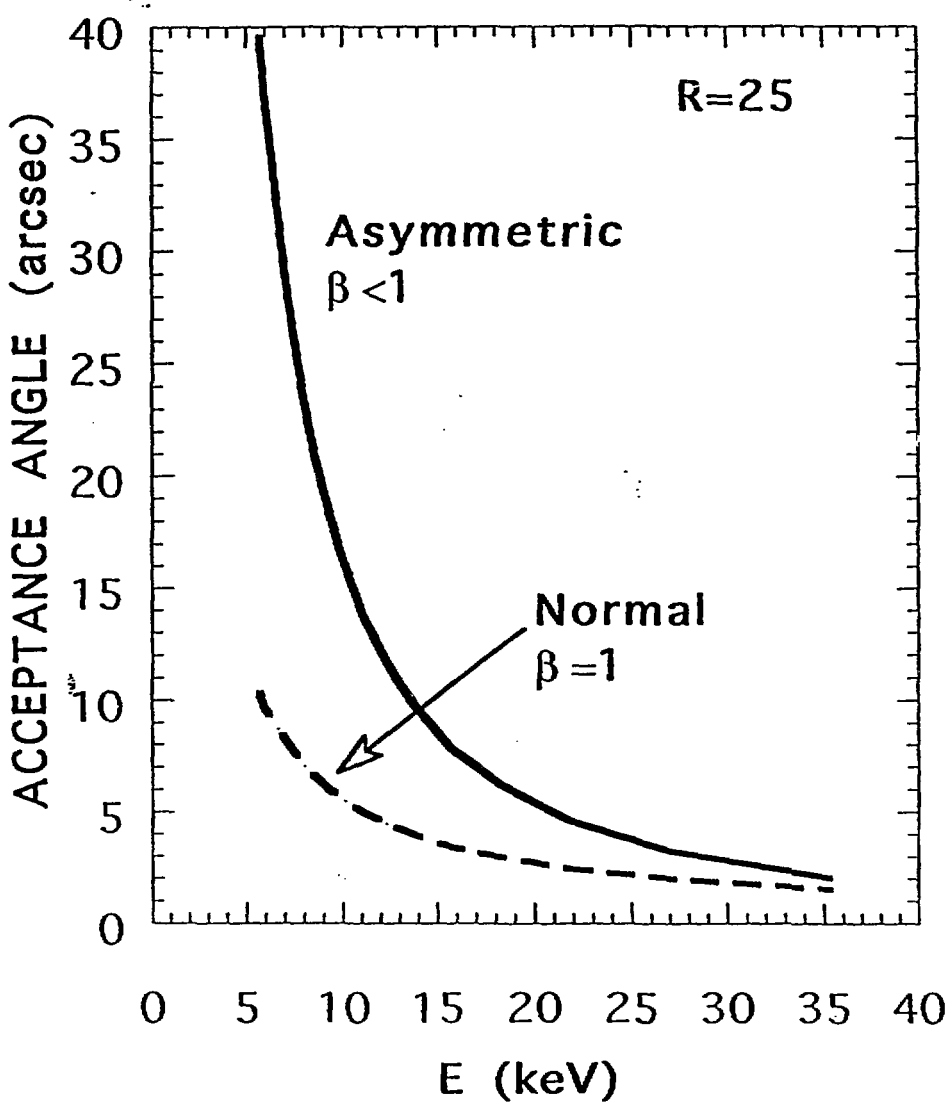
R=25
Asymmetric
β <1
Normal
β =1
ACCEPTANCE ANGLE (arcsec)
E (keV)
0
5
10
15
20
25
30
35
40

Fig 8

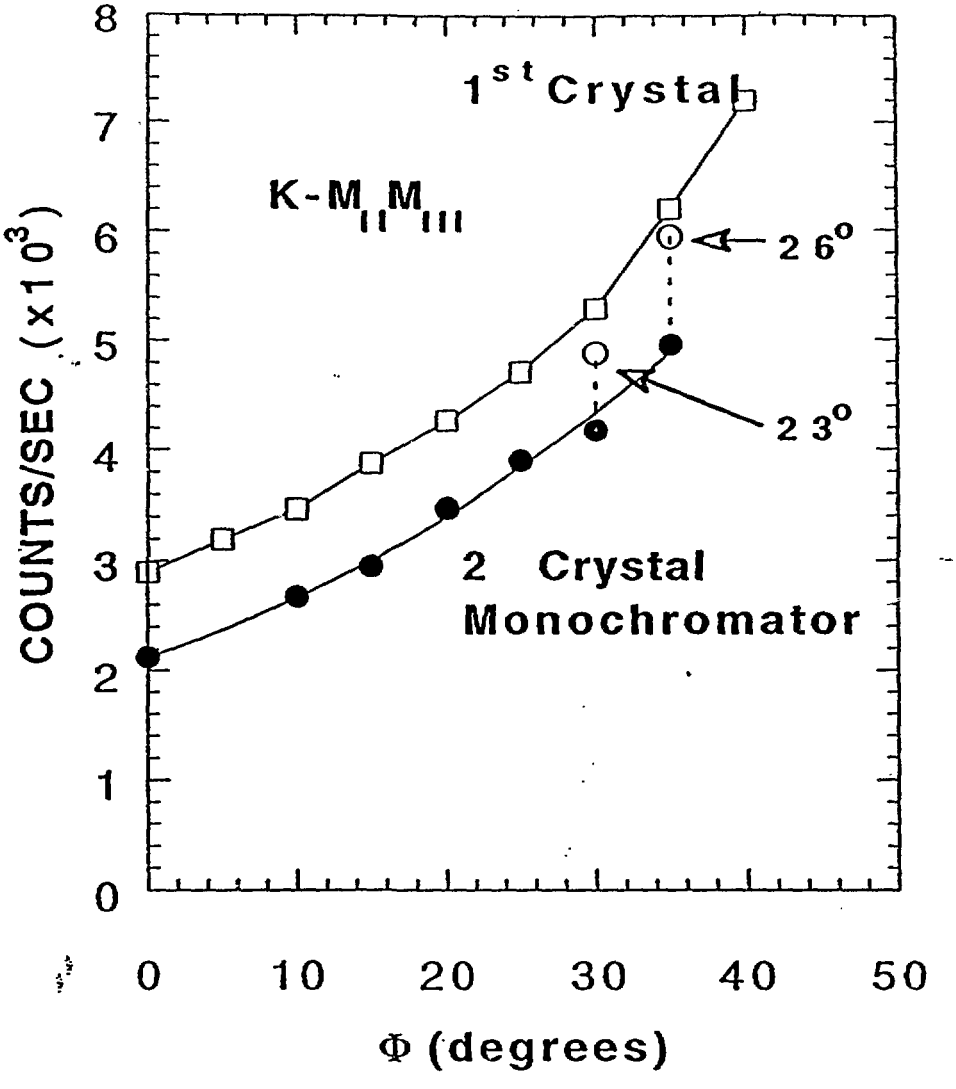

Rotation about axis ⊥ to crystalline planes

Fig 9

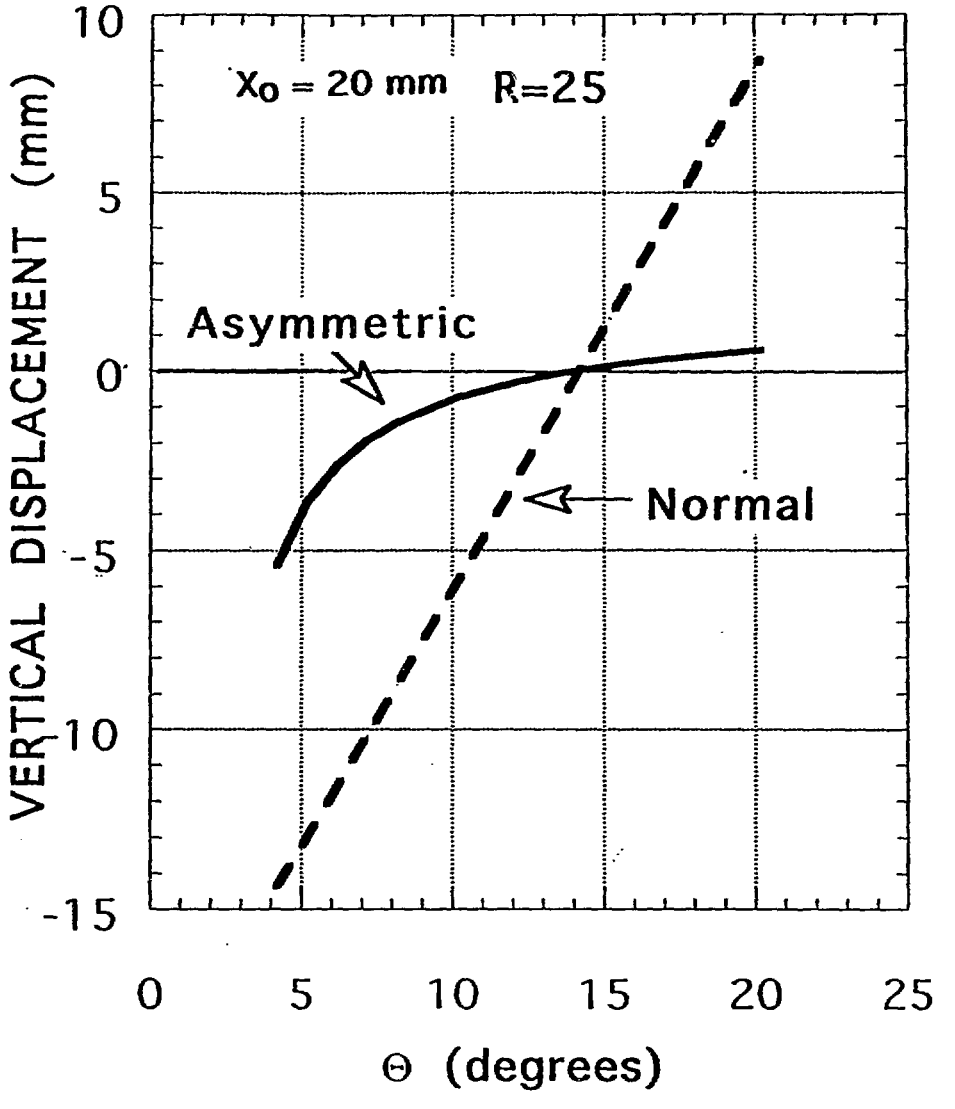
X_o = 20 mm
R=25
Asymmetric
Normal
VERTICAL DISPLACEMENT (mm)
10
5
0
-5
-10
-15
0
5
10
15
20
25
Θ (degrees)

Fig 10